Metastable Underwater Superhydrophobicity

Rosa Poetes, Kathrin Holtzmann, Kristian Franze, and Ullrich Steiner*

Cavendish Laboratory, University of Cambridge, Cambridge CB3 0HE, United Kingdom

(Received 13 July 2010; published 14 October 2010)

Superhydrophobicity is generally considered to be a thermodynamically stable wetting state. The stability of the plastron (the thin air film separating the substrate from the water in the superhydrophobic state) was studied in underwater experiments. The plastron exhibited a rapid decay after a well defined onset time, which was found to be dependent on the immersion depth. The plastron decay is explained in terms of a model, which is based on confocal microscopy measurements. The limited underwater plastron stability explains the rarity of permanently submerged superhydrophobic surfaces in nature and limits their scope for commercial applications.

DOI: 10.1103/PhysRevLett.105.166104 PACS numbers: 68.08.Bc, 47.55.D−, 68.03.−g, 68.35.Ct

Complete water repellency has fascinated scientists and laymen alike for more than a century [1]. Triggered by botanical studies [2], there has been a renewed interest in this phenomenon, both fundamentally as well as in terms of technological applications [3]. The wetting of liquids on rough surfaces has been explained in terms of a balance of the interfacial free energies of the three involved media (substrate, liquid, vapor) by Wenzel [4] and Cassie and Baxter [5]. Two wetting states have a minimum in the free energy landscape [6]: Wenzel wetting is characterized by a complete contact of the liquid with all microscopic surface features, while in Cassie-Baxter (CB) the wetting liquid makes contact only with a small area fraction of protruding roughness peaks, trapping an air film (plastron) between the liquid and the substrate. These two wetting states often coexist on the same substrate. The relative value of the free energy minima and the barrier between them depends on the chemical nature of the surface, the detailed surface topography, and the wetting liquid.

In the case where CB wetting forms the lowest free energy state, the plastron is expected to be energetically stable [7]. Interestingly, however, superhydrophobic surfaces in nature are found almost exclusively on surfaces that are only intermittently exposed to water. With the exception of a rare species of floating ferns [8] and spiders, which use plastron air bubbles to breath [9], underwater superhydrophobicity is absent. Herminghaus [10] has observed the disappearance of the plastron of the superhydrophobic *Cotinus coggygria Scop*. upon complete immersion of the leaf to a depth of 20 cm for several seconds. Yet, underwater superhydrophobicity is thought to be technologically valuable, e.g., for drag, reduction and the prevention of underwater fouling [11]. Surprisingly, systematic studies of plastron underwater stability are rare [12–14].

The CB model and later descriptions based on the CB argument are correct only under the usual wetting assumptions, that is, for the case where the three involved phases are in thermodynamic equilibrium. While this is a good approximation when performing experiments with small amounts of liquids (e.g., drops) in an equilibrated (confined) vapor volume, ambient water and air are only very seldom in thermodynamic equilibrium: the solubility of air in water (≈ 23 mg/l at 25 °C) varies strongly with temperature and depends on other parameters, such as the agitation of water or biological activity. It is therefore interesting to reexamine plastron stability under realistic wetting conditions, permitting liquid-vapor exchange.

Here, we report a study on the underwater stability of plastrons on superhydrophobic Teflon surfaces. Samples were prepared by roughening 5×5 cm^2 Al plates by bead blasting, followed by spray-coating a primer (DuPont 459–804) and a Teflon suspension (DuPont 852–200) [15]. This resulted in very rough surfaces with high static contact angles ($155° < \theta_{\text{static}} < 168°$). Measurements were also performed on *Nelumbo Nucifera* (lotus) leaves.

Figures 1(a)–1(d) show scanning electron microscopy (SEM) images comparing superhydrophobic Teflon [Fig. 1(a) and 1(c)] to the top surface of a dried lotus leaf [Fig. 1(b) and 1(d)]. The two samples are morphologically extremely similar. They both consist of micrometer-sized protrusions [Figs. 1(a) and 1(b)] with a ~ 10 μm spacing and a 10–50 nm-sized fine texture [Figs. 1(c) and 1(d)], reflecting the crystalline nature of the two surface materials (polytetrafluoroethylene and epicuticular wax, respectively). Despite the different intrinsic wettabilities of the two surface materials, both surfaces display a similar superhydrophobic effect, with static contact angles around 160°.

Samples were mounted on a sample holder at 45° and submerged in a home-built glass water tank at varying depth h. The reflection of light from the plastron gives the samples a silvery appearance, which was observed by a horizontally mounted camera under optimized illumination and exposure conditions. Care was taken to prevent the change of theses parameters with time. Prior to each experiment the tank was filled with deionized water (15 MΩ resistance) and the samples were inserted after 10 min, keeping the water stationary for the remainder of the

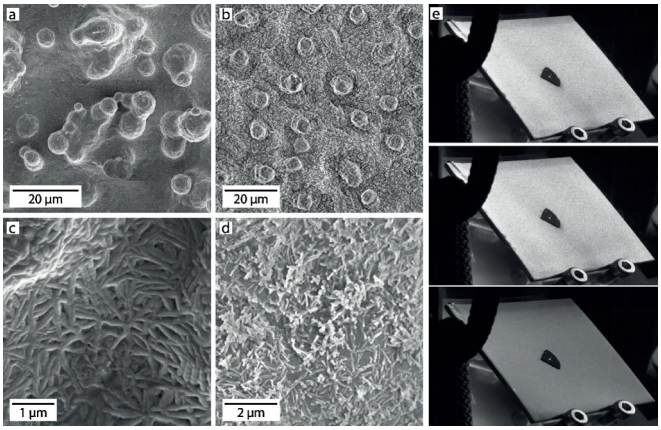

FIG. 1 (color online). SEM images of sprayed-on Teflon (a),(c) and a lotus leaf (b),(d) surfaces, showing sparse micrometer-sized protrusions (a),(b), separated by a sub-100 nm secondary structure. The image series in (e) shows the reflection of immersed 5×5 cm^2 samples at a depth of $h = 126$ cm for 30 min, 35 min, and 60 min, visualizing the decay of the plastron with time. The dark spot on the center of the sample was used to provide a brightness reference, allowing us to keep the image exposure condition constant.

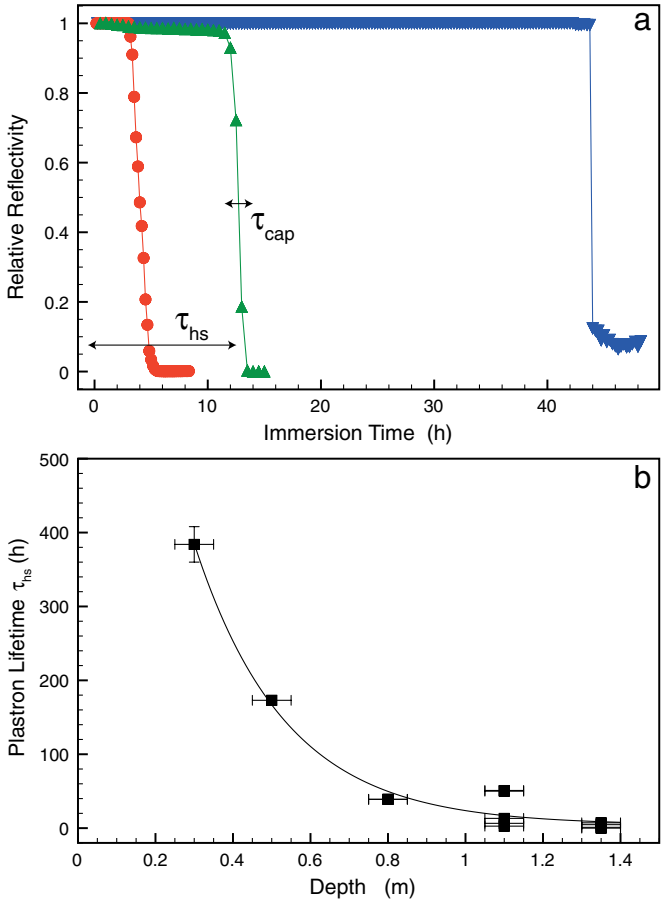

FIG. 2 (color online). (a) Plastron reflectivity for immersion depth of 0.5 m (▼), 1.1 m (▲), and 1.3 m (●). τ_{hs} and τ_{cap} are the characteristic times quantifying the two plastron decay regimes. (b) Plastron lifetime τ_{hs} as a function of immersion depth (the depth-error bars arise from the evaporation of water during the experiment). The solid line is a fit to an exponential function.

experiment. Images of the samples were taken at regular intervals of 5 min $< \Delta t <$ 15 min. A typical sample series is shown in Fig. 1(e). The images were converted to 8-bit gray scale and a threshold was applied, which was kept fixed for the entire image series. A coarse-grained reflection intensity defined as the bright vs dark pixel count of an appropriate region of interest was used as a measure for the relative coverage of the sample by the plastron.

Figure 2(a) shows typical data sets for three immersion depths. All samples had a characteristic onset time during which no optical change of the samples could be detected, followed by a rapid decay of the plastron. The decay of the plastron typically occurred homogeneously over the entire sample surface. The characteristic plastron decay time τ_{hs} was defined as the time for which the intensity was 10%. Figure 2(a) shows the strong dependence of τ_{hs} with immersion depth h of the sample. The samples at low values of h exhibited a weak reflecting shimmer (estimated residual reflection of 5%–10%) after plastron decay, which was much less pronounced for samples deeper in the tank. Figure 2(b) shows the variation of τ_{hs} with h. The strongly nonlinear variation of $\tau_{hs}(h)$ is best fitted by an exponential decay. While the results are reproducible for the chosen approach, it is important to note that τ_{hs} depends also on other parameters of the water. The circulation of water in the tank or the use of water that has been stored in the tank for several days prior to the experiments yielded much shorter values of τ_{hs}.

Confocal microscopy was used to elucidate the origin of plastron decay. Figures 3(a) and 3(b) show a sample immediately after immersion and after laser scanning for 15 min. The plastron consisted initially of a continuous air layer that is supported by a very sparse distribution of pinning points, decaying into a state where a small distribution of air bubbles are pinned to the surface. The plastron lifetime in the confocal experiment was much reduced compared to the water tank experiment, which presumably is caused by the much smaller water volume and the local heating by the scanning laser. Rather than continuously monitoring the sample by confocal microscopy, samples were instead incubated in a separate water volume for varying periods of time before microscopy measurements. The plastron of a sample after immersion for 5 days in Fig. 3(c) is much less bright and is supported by more pinning points. Cross sections for plastrons after fresh immersion and after 1 h incubation are shown in Figs. 3(d) and 3(e). The thickness of the plastron layer was found to depend on the immersion time, reducing from 70 μm in Fig. 3(d) to 50 μm Fig. 3(e). Eventually the plastron decays to form locally pinned bubbles shown in Fig. 3(f).

The combined results of the immersion and confocal microscopy experiments allow us to devise a model of

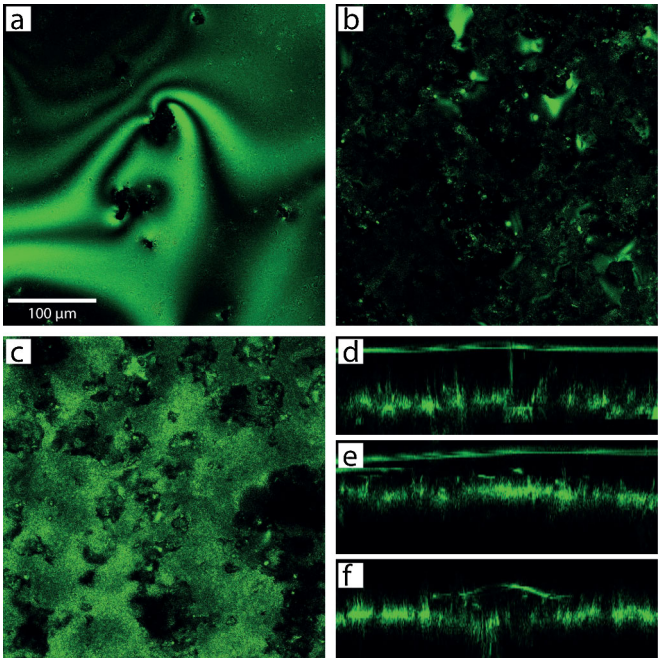

FIG. 3 (color online). Confocal microscopy images and cross sections of the plastron, taken in reflection mode. Surface images of freshly immersed sample surfaces after scanning for (a) 15 min, and (b) 30 min, showing a complete plastron and localized air bubbles, respectively. (c) In-plane slice of the plastron close to the air-water interface after immersion for 5 days, showing the increased number of surface-water contact points. The cross sections in (d),(e) show plastrons of a freshly immersed sample (d) and after immersion for 1 h (e), with plastron thicknesses of $\approx 70\ \mu$m and ≈ 50 m, respectively. The decay of the plastron to spherical cup-shaped bubbles after extended laser scanning is shown in (f).

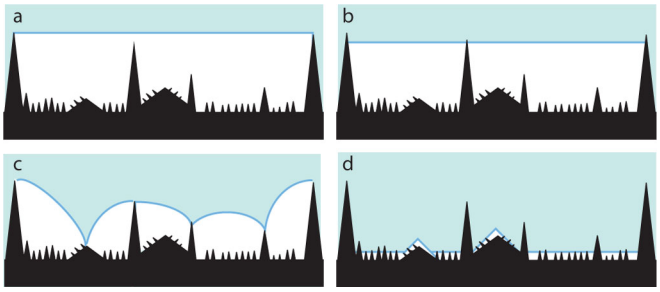

FIG. 4 (color online). Schematic of plastron decay. The initially $\sim$100 μm-thick air layer is only sparsely supported by surface protrusions (a). As the layer thins by diffusion of air into water, an increasing number of surface protrusions make contact with water (b). Eventually the homogeneous air layer breaks up and forms spherical cup-shaped air bubbles, which rapidly dissolve in water, driven by the increasing Laplace pressure (c). Finally, only a very thin secondary plastron remains, which spans the secondary surface structure of Figs. 1(c) and 1(d).

plastron stability. Initially the plastron is about 100 μm thick and only the highest surface protrusions are in contact with water [Fig. 4(a)]. With time the plastron thins by diffusion of air into the surrounding water. Because of the random topography of the surface, an increasing number of surface features come into contact with the plastron [Fig. 4(b)]. Since the planar liquid-air surface stays intact and due to the high liquid-air reflectivity, this does not cause a macroscopically observable change in light reflectivity, leading to the plateau in Fig. 2(a).

The mass flux j of air (N_2) into water is limited by the gas mass transfer coefficient into water k_l and can be approximated

$$j = k_l\left(\frac{p}{H} - c\right), \tag{1}$$

where c is the gas concentration in water and H is Henry's constant [16]. Initially the plastron is planar, the Laplace pressure is zero, and the air mass transfer into water and therefore the plastron lifetime τ_{hs} is dominated by the hydrostatic pressure of the water column of density ρ at depth h, $p(h) = p_0 + \rho g h$, with p_0 at atmospheric pressure and g the gravitational constant. For an ideal gas, $(\partial \ln f/\partial p)_{T,c} = \bar{v}/(RT)$, where f is the fugacity, $\bar{v}$ is the partial molar volume, R is the gas constant, c the dissolved gas concentration, and T the temperature [17,18]. Integration between two hydrostatic pressures and substituting the equilibrium partial pressures p' for the fugacities result in [17]

$$\ln\left(\frac{p'}{p'_0}\right) = \frac{\bar{v}}{RT}[p(h) - p_0]. \tag{2}$$

Equation (2) implies an exponential variation of mass transfer from the plastron into water with increasing h, reflecting the exponential decrease in τ_{hs} in Fig. 2(b).

As diffusion proceeds, the direct substrate-water contact increases, until part of the surface is substantially wetted by water and the plastron breaks up into spherical cup-shaped air bubbles that are pinned to the surface [Fig. 4(c)]. At this point the Laplace pressure $p_L = 2\gamma/r$ (with γ the water surface tension and r the radius of curvature) becomes important. The breakup of the film into spatially distinct bubbles and their Laplace-pressure driven dissolution causes the rapid decay in reflectivity in Fig. 2(a).

The diffusion of air from the spherical caps is similar to the dissolution of free air bubbles in water as discussed by Epstein and Plesset [19] and Ljunggren [20]. Using the ideal gas law, a variation of the Epstein-Plesset [19] equation yields the lifetime of spherical caps

$$\tau_{\mathrm{cap}} = \frac{B_0 H r_0^3 p'(h)}{8RTD\gamma}. \tag{3}$$

B_0 is the fractional volume of the spherical cap compared to a complete sphere ($\sim 10^{-2}$), D is the diffusion coefficient of air (N_2) in water, and r_0 is the initial bubble radius. In Fig. 2(a), τ_{cap} signifies the characteristic time for the rapid decrease in reflection. For a typical value of $r_0 \approx 100\ \mu\mathrm{m}(h \sim 0)$, $\tau_{\mathrm{cap}} \sim 2$ h, in agreement with the results

of Fig. 2(a). This is a clear qualitative indication that the late-stage decay of the plastron is dominated by the Laplace pressure of the decaying surface-attached bubbles. The variation of τ_{cap} with p' should give rise to an exponential variation of the profile broadening in Fig. 2(a), but this was not further investigated.

Careful scrutiny of sample reflectance and confocal microscopy images reveal a very thin residual air layer on the samples after complete plastron decay, particularly for samples at low immersion depth h. It is likely that this secondary plastron is connected to the hierarchical structure of the surfaces in Fig. 1(a), schematically shown in Fig. 4(d). Following the arguments presented above, such a thin air layer should be extremely short lived. While, qualitatively, the secondary plastron was observed only for small values of h, it is possible that additional stabilizing effects are necessary to explain the stability of this thin air layer. Samples with or without a secondary plastron, when removed from water, exhibited Wenzel-type wetting with a water contact angle of $\sim 120°$ and a large contact angle hysteresis.

In summary, we have investigated the lifetime of superhydrophobic plastrons on rough Teflon surfaces upon immersion into water. Macroscopic optical imaging and confocal microscopy revealed a characteristic, depth dependent lifetime of the plastron, which is explained in terms of a two-stage decay. During the first stage, the air layer thins by diffusion of air into water. The exponential depth dependence of the plastron arises from an exponential variation of the partial vapor pressures of the gases in the plastron with hydrostatic pressure, resulting in an exponential increase in the diffusion of air into water with increasing depth. Once the plastron reaches a critical thickness, it decays into spherical cup-shaped air bubbles. Driven by the Laplace pressure these bubbles rapidly dissolve in water, as explained by the Epstein-Plesset equation.

Our study contradicts the common belief that the plastron is thermodynamically stable. In difference to earlier approaches assuming the coexistence of the liquid and vapour phases, our experiment considers the more realistic case of stagnant water in an open environment. Non-equilibrium studies, such as the work presented here, suffer from the complication of properly defining the experimental system. In the experiments presented here, aerated water continuously outgasses throughout the duration of the experiment. Preliminary studies showed that the plastron lifetime was reduced when using water that had been outgassed for different periods of time. Also, flowing water strongly reduced the plastron lifetime, suggesting the influence of hydrodynamic parameters. In addition to the presented quantitative study, these qualitative observations confirm a relatively short lifetime of plastron even for relatively shallow immersion depths. Further preliminary studies on other superhydrophobic surfaces confirm the findings reported here, but the plastron decay time varied. For example, the plastron lifetime of a lotus leaf immersed to depth of 55 cm was only ~ 1 h, leaving a clearly visible, longer lived secondary air film. This suggests that the primary plastron lifetime varies with the nature of the superhydrophobic surface (i.e., its structural details and its surface energy). While more experimental studies are needed to fully characterize plastron decay, our findings are interesting when considering superhydrophobicity in nature and they are potentially important for the technological exploitation of this effect.

EPSRC funding (EP/E022561) is gratefully acknowledged. KF acknowledges the Alexander von Humboldt Foundation. This work was triggered by discussions with Cambridge Enterprise.

*u.steiner@phy.cam.ac.uk

[1] C. V. Boys, *Soap Bubbles* (Society for Promoting Christian Knowledge, London, 1902).
[2] C. Neinhuis and W. Barthlott, Ann. Bot. **79**, 667 (1997).
[3] M. Callies and D. Quéré, Soft Matter **1**, 55 (2005).
[4] R. N. Wenzel, Ind. Eng. Chem. **28**, 988 (1936).
[5] A. B. D. Cassie and S. Baxter, Trans. Faraday Soc. **40**, 546 (1944).
[6] A. Tuteja *et al.*, Science **318**, 1618 (2007).
[7] A. Marmur, Langmuir **22**, 1400 (2006).
[8] W. Barthlott *et al.*, Adv. Mater. **22**, 2325 (2010).
[9] M. R. Flynn and J. W. M. Bush, J. Fluid Mech. **608**, 275 (2008).
[10] S. Herminghaus, Europhys. Lett. **52**, 165 (2000).
[11] K. Koch and W. Barthlott, Phil. Trans. R. Soc. A **367**, 1487 (2009).
[12] H. Rathgen *et al.*, Phys. Rev. Lett. **99**, 214501 (2007).
[13] L. Lei *et al.*, Langmuir **26**, 3666 (2010).
[14] H. Rathgen and F. Mugele, Faraday Discuss. **146**, 49 (2010).
[15] P. van der Wal, Soft Matter **3**, 426 (2007).
[16] E. L. Cussler, *Diffusion, Mass Transfer in Fluid Systems* (Cambridge University Press, Cambridge, England, 1997).
[17] T. Enns, P. F. Scholander, and E. D. Bradstreet, J. Phys. Chem. **69**, 389 (1965).
[18] H. Ludwig and A. G. Macdonald, Comp. Biochm. Physiol., Part A, Mol. Integr. Physiol. **140**, 387 (2005).
[19] P. S. Epstein and M. S. Plesset, J. Chem. Phys. **18**, 1505 (1950).
[20] S. Ljunggren and J. C. Eriksson, Colloids Surf. **129–130**, 151 (1997).